Enhanced Propagation for Relativistic Laser Pulses in Inhomogeneous Plasmas Using Hollow Channels

J. Fuchs,[1,2,*] E. d'Humières,[2,3,4] Y. Sentoku,[2] P. Antici,[5] S. Atzeni,[5] H. Bandulet,[1] S. Depierreux,[6] C. Labaune,[1] and A. Schiavi[5]

[1]*LULI, École Polytechnique, CNRS, CEA, UPMC, route de Saclay, 91128 Palaiseau, France*
[2]*Physics Department, MS-220, University of Nevada, Reno, Nevada 89557, USA*
[3]*Centre de Physique Théorique, École Polytechnique, CNRS, 91128 Palaiseau, France*
[4]*CELIA, UMR 5107 Université Bordeaux I-CNRS-CEA, 351 Cours de la Libération, 33405 Talence, France*
[5]*Dipartimento SBAI, Università di Roma "Sapienza" and CNISM, Via Scarpa 14, 00161 Roma, Italy*
[6]*CEA, DAM, DIF, F-91297 Arpajon, France*

(Received 25 June 2009; published 24 November 2010)

The influence of long (several millimeters) and hollow channels, bored in inhomogeneous ionized plasma by using a long pulse laser beam, on the propagation of short, ultraintense laser pulses has been studied. Compared to the case without a channel, propagation in channels significantly improves beam transmission and maintains a beam quality close to propagation in vacuum. In addition, the growth of the forward-Raman instability is strongly reduced. These results are beneficial for the direct scheme of the fast ignitor concept of inertial confinement fusion as we demonstrate, in fast-ignition-relevant conditions, that with such channels laser energy can be carried through increasingly dense plasmas close to the fuel core with minimal losses.

DOI: 10.1103/PhysRevLett.105.225001 PACS numbers: 52.35.Mw, 52.38.Dx, 52.38.Hb, 52.65.Rr

The ability to propagate short (pulse duration $<$ps), ultraintense laser pulses over long distances in plasmas is crucial for a number of applications such as compact laser wakefield electron accelerators [1], x-ray lasers [2], and fast ignition (FI) of inertially confined fusion targets [3]. In FI, an intense laser pulse is used to generate particles, close to a precompressed thermonuclear fuel, to ignite it.

Several options [4] are currently pursued for FI. Direct target irradiation by the intense pulse has been studied [5–7]. The laser pulse is, however, subject to losses occurring in the coronal plasma surrounding the core [8]. To prevent this, an alternate scheme using a cone embedded in the target [9] has been proposed to provide a path clear of plasma for the laser pulse. It, however, yields a lesser fuel compression due to the inherent target asymmetry [5]. Other issues of this scheme are (i) the high levels of laser energy before the main pulse filling the cone with plasma and affecting the laser-cone coupling [10] and (ii) fuel-cone mixing during the implosion [11].

A clear path for the igniting laser pulse could alternatively be provided, as originally proposed [3] and more recently highlighted by simulations [6,12], by a channel predrilled in the inhomogeneous fuel coronal plasma. Allowing avoidance of the drawbacks of the cone scheme, it would be formed by using an auxiliary laser pulse, short [4,13,14] or long [15]. Channels have shown to be effective to guide [1,16] intense laser pulses and minimize coupling with detrimental instabilities [7], albeit only in low-density, homogenous plasmas [17]. Their use for FI was, however, not experimentally explored up to now.

In this Letter, by coupling measurements and simulations, we demonstrate efficient energy transport of relativistic laser pulses using preformed channels bored through nonuniform, inhomogeneous low-density plasmas that correspond to the corona of planned imploded FI targets. Not only is the transmission at the laser wavelength increased by a factor of >3 compared to when the relativistic pulse bores its own propagation channel in such coronal plasmas, but a vacuumlike beam quality is also maintained. We also observe a strong reduction of the forward laser-plasma instabilities. Thus more energy could be delivered to an FI target high-density absorption point. Applying the channel drilling scheme to a FI target without a cone would then allow fully symmetric compression of the capsule [5] and minimize the losses for the igniting pulse through the corona.

The experiment was performed by using the 100 TW short pulse laser at the Laboratoire pour l'Utilisation des Lasers Intenses. Four different beams optically split from the main line were used. A first pulse at $\lambda = 1.053$ μm (or 1ω), uncompressed (450 ps FWHM duration), is focused, by using a random phase plate, at an intensity of 10^{13} W $\cdot$ cm^{-2} and at 45° on a thin 0.3 μm CH target that is exploded to create a background inhomogeneous plasma. Depending on the time elapsed after this irradiation, various configurations for this plasma can be explored, as given in Table I. The plasma parameters are inferred by comparing the measured density profile to two-dimensional (2D) hydrodynamic simulations performed with the code DUED [18]. The plasma density measurement was made by an optical probe. For this, a second pulse, low

 © 2010 The American Physical Society

TABLE I. Parameters of the background plasma explored in the experiment (without a channel or interaction beam).

Peak background plasma density n_e^0 (cm^{-3})	Main gradient scale length L (μm)	Density at the beams focus point (cm^{-3})
2.2×10^{20}	115	8×10^{19}
10^{20}	150	8×10^{19}
6×10^{19}	300	4.5×10^{19}
4×10^{19}	375	3×10^{19}
10^{19}	545	6×10^{18}

energy, compressed (400 fs), and frequency-tripled to 351 nm, is used as a transverse probe and sent into a Nomarski interferometer. A density profile along the x direction, the expansion axis, and corresponding to the center of the plasma for one of the configurations can be seen in Fig. 1(a). The central region of the profile cannot be accessed by the measurement due to the refraction of the optical probe beam. Overlaid is the density profile in the corona of an ignition-designed target for the planned High Power Laser Energy Research (HiPER) large-scale FI facility [19]. Our plasma conditions correspond quite well to the corona of such an FI imploded target, showing the relevance to FI of the millimeter-long background plasmas used here. We constrain our plasmas to be fully underdense, i.e., below the critical density $n_c[\mathrm{cm}^{-3}] = 10^{21}/\lambda^2[\mu\mathrm{m}]$, so that the propagation of an intense laser pulse through it can be studied.

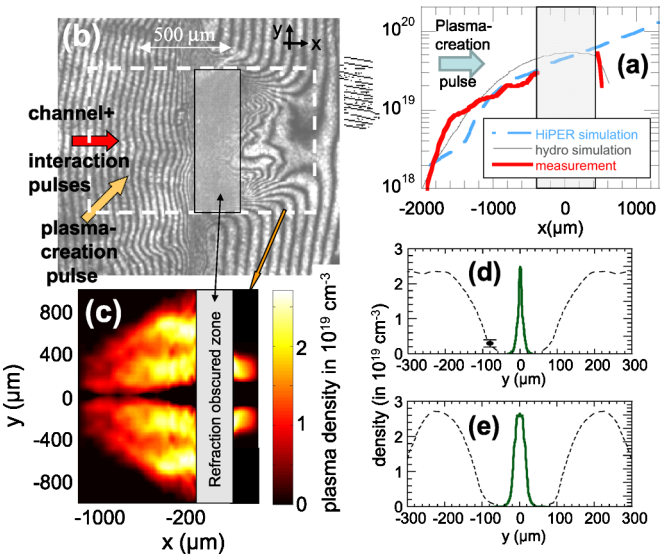

FIG. 1 (color online). (a) Measured (thick line) and simulated (thin line) on-axis electron density profile for one of the explored background plasma configurations given in Table I (3rd line of the table). The front part (facing the incident laser pulse) of the plasma gradient can be fitted by $\exp(-x/L)$. L is given in Table I. Overlaid is the coronal plasma profile of a nominally compressed target designed to be used in the HiPER FI facility (dashed line). (b) Interferogram recorded in the case where the channel beam was injected into the background plasma; the time corresponds to 50 ps after the peak of the channel beam. (c) Density map extracted from (b) by Abel inversion. (d) Lineout (dashed line) of (c) at the left side of the inaccessible zone [shown in (a)–(c) by a gray bar] and transverse profile of the interaction beam at this point (thick line). (e) The same as (d) but at the right side of the inaccessible zone.

In any given plasma configuration, a third pulse ("channel pulse") can be injected on the long gradient side of the target to create a hollow density channel [15], as shown in Figs. 1(b) and 1(c). For all configurations, when this pulse is on, the channel is bored, by ponderomotive expulsion of electrons, followed by the ions [15], through the plasma, with a diameter ~ 200 μm [see Figs. 1(d) and 1(e)]. We stress that the channel is not limited in length but is bored throughout the whole background plasma [see Fig. 1(c)]. Note that the density at the channel bottom is evacuated to within the precision of the interferometer ($\sim 5 \times 10^{17}$ cm^{-3}). The channel pulse is also at $\lambda = 1.053$ μm and uncompressed. This last point is of interest since using such a long pulse (rather than a short one) for channel drilling relaxes the constraints imposed on the laser facility. It is focused by using a $f/3$ off-axis parabola over 13 μm FWHM (achieving 10^{16} $\mathrm{W \cdot cm^{-2}}$) and 250 μm in front of the initial target. The latter position is the most efficient at boring the channel.

Finally, a fourth pulse, the intense interaction pulse, is sent into the plasma, from the same side of the plasma, with or without a channel. It is short (320 fs), frequency-doubled to 526 nm (or 2ω), and focused to 11 μm FWHM [as shown in Fig. 1(d)] with 55% of the energy in the central peak, achieving a peak intensity of 3×10^{18} $\mathrm{W \cdot cm^{-2}}$. It is also focused 250 μm in front of the initial target. Its Rayleigh length in vacuum is ~ 100 μm, much shorter than the plasma or channel longitudinal scale lengths, allowing us to test appropriately propagation over such a long range. When it is used in conjunction with the channel pulse, the temporal peaks of the two pulses are made to coincide. As both pulses use the same parabola, the interaction pulse is naturally aligned into the plasma channel. The overlap between the channel and interaction focal spots is verified with ~ 2 μm precision. Before each shot, a deformable mirror [20], correcting any wave front deformation, ensures that both pulses are optimally focused. Forward scattering and transmitted light after the plasma are collected on-axis by using an uncoated $f/1.5$ off-axis parabola and sent to near-field, far-field, and absolutely calibrated spectral diagnostics.

Figure 2(a) shows that boring a channel in the background plasma significantly helps in transporting the energy of the interaction pulse through the coronal plasma. For all configurations, the interaction pulse transmitted energy recorded at $\lambda = 526 \pm 10$ nm is indeed increased by a factor of >3 when adding a channel. We are confident that the observed increase of the 2ω light in the presence of

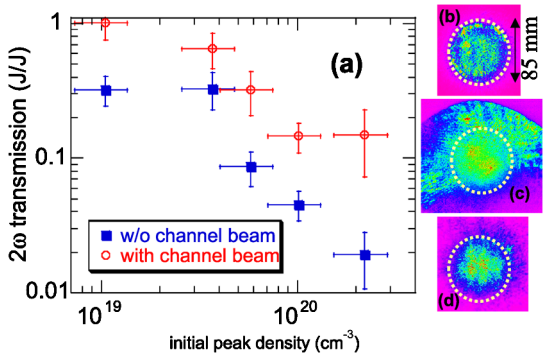

FIG. 2 (color online). (a) Time-integrated transmitted energy at $\lambda = 526$ nm for 10 J average incident energy of the interaction pulse as a function of the peak density of the background plasma ($n_e{}^0$). (b) Near-field profile of the transmitted interaction beam propagating in vacuum; (c) the same for propagation in a plasma with $n_e{}^0 = 4 \times 10^{19}$ cm^{-3}; (d) the same for propagation in a hollow channel bored in the same plasma. The dotted lines in (c) and (d) represent the contour of the vacuum profile.

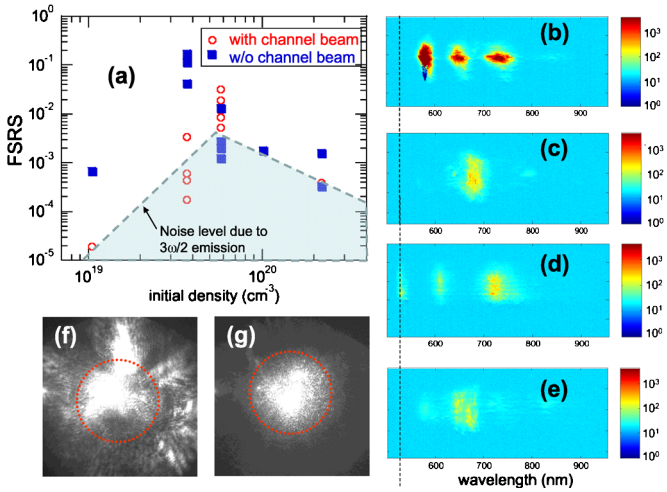

FIG. 3 (color online). (a) Fraction of the interaction pulse energy contained in the FSRS as a function of the peak density of the unperturbed plasma. (b) FSRS spectrum for $n_e{}^0 = 4 \times 10^{19}$ cm^{-3} and without the channel beam. The dashed line represents the 526 nm wavelength of the interaction beam, attenuated on purpose. (c) The same with the channel beam on. (d),(e) The same as (b),(c) for $n_e{}^0 = 6 \times 10^{19}$ cm^{-3}. (f) Near-field profile of the FSRS light filtered in a 570–680 nm band without a channel and for $n_e{}^0 = 4 \times 10^{19}$ cm^{-3}; (g) the same but with a channel. The dotted circle corresponds to the size of the laser vacuum profile, as in Fig. 2(b).

the channel beam is not due to frequency conversion of the channel pulse in the plasma and/or channel. Indeed, firing the channel pulse showed only $\ll 0.1$ J of light converted at 2ω (compared to the 10 J interaction beam), consistently with other measurements [21]. The interaction beam is not only better transmitted through the plasma using the channel, but its propagation mode is also maintained close to the vacuum mode, as can be seen by comparing Figs. 2(b) and 2(d). On the contrary, in the absence of the channel, the beam is observed to spread widely, as seen in Fig. 2(c). Similar results as those shown in Figs. 2(c) and 2(d) are obtained in all configurations.

Propagating the interaction pulse into the channel also alleviates energy loss into instabilities. Such instabilities not only redistribute light in other modes but can also produce hot electrons, through forward-Raman scattering (FSRS) [22] ahead of the fuel dense core. Being divergent, these electrons cannot contribute as efficiently as electrons generated at the dense core interface to heating the imploded core. FSRS is thus doubly detrimental for FI. Without channel, FSRS from the interaction pulse is clearly observed in the form of sideband frequencies $2\omega \pm \omega_p$, $2\omega \pm 2\omega_p$, etc. (where ω_p is the plasma frequency); see Figs. 3(b) and 3(d). However, as shown in Figs. 3(c) and 3(e), the spectrum, recorded in the presence of the channel, no longer presents discernible harmonics and peaks at ~670–680 nm, regardless of the peak background plasma density. This signal corresponds well to $3\omega/2$, which suggests that it is generated by two-plasmon decay [22] near $n_c/4$. It is likely to have been produced by the long channel pulse when it encountered such densities during its temporal evolution. This is confirmed by our 2D hydrodynamic simulations. This signal is dominant in the presence of the channel and is lower than the FSRS measured without the channel [see Fig. 3(a)]. It thus shows that, with the added channel, FSRS generated by the interaction pulse is quenched. This effect is likely linked to the intrinsic effect of the channel structure, as predicted in Ref. [23]. The modification of the FSRS angular structure by the channel is another evidence of the channel guiding ability. It is a widely spread structure in the absence of a channel [see Fig. 3(f)], whereas with channel, although the FSRS is reduced, its structure is more regular, close to that of the interaction beam [see Fig. 3(g)].

Simulations of the intense laser-plasma interaction using the 2D particle-in-cell code PICLS [24] meet our observations and show furthermore that detrimental FSRS-linked electron generation is significantly decreased in the presence of the channel. The simulation box is 150 μm long and 100 μm wide, with a mesh size $\Delta x = \Delta y = 50$ nm and 10 particles per species per cell. The time step is equal to 1.65×10^{-1} fs. Overall, the laser propagates, along the x direction, 500 μm into the plasma, and we use a moving window to follow the propagating laser pulse. For the laser, the parameters follow the experimental conditions: 0.5 μm wavelength, 3×10^{18} W/cm^2 intensity, 350 fs pulse duration, and 11 μm FWHM transverse spot size. The laser is focused 150 μm after its entrance into the fully ionized protons and electrons plasma that is reached 150 fs after the beginning of the calculation. The incidence is normal to the plasma surface, with the laser electric field in the simulation plane. The plasma is initially located 10 μm from the laser entrance side of the box. Its density

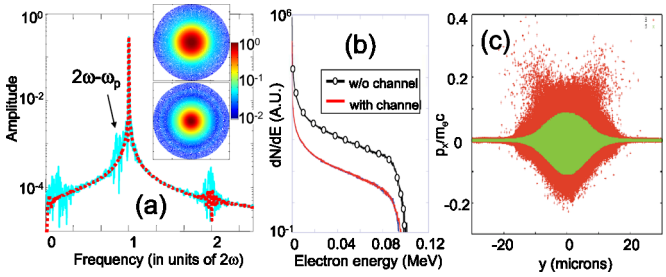

FIG. 4 (color online). (a) Simulated spectra of the electromagnetic waves within the simulation box 2.05 ps after the entrance of the maximum of the pulse in the plasma for the cases with (red dots) and without a channel (blue line). The main peak corresponds to the laser field. Inset: Simulated near-field profile of the transmitted interaction beam after propagation in the plasma (top) without a channel and (bottom) with a hollow channel bored in the same plasma. The near fields are obtained by Fourier transform of the focused laser beam. (b) Simulated electron energy spectra for the case with a high density and no channel and the case with a channel. (c) Simulated transverse electron phase space (p_x as a function of y) for the case with a high density and no channel (in red) and the case with a channel (in green). Both are recorded 1.5 ps after the entrance of the maximum of the pulse in the plasma.

is constant at 10^{19} cm^{-3} in the case without a channel. In case with a channel, to model it, the longitudinal plasma density profile is constant, but the transverse density profile is a parabola fitting the measurement shown in Fig. 1(d) and 1(e), i.e., with $n_e(y) = 10^{18} \times [1 + 5 \times 10^{-4}(y\text{-}y_0)^2]$ in units of cm^{-3}, where y is in micrometers and y_0 is the middle of the box.

In the simulations, in the case with a channel, the spectrum of the propagated laser is maintained close to the vacuum case. However, in the case without a channel, similar to the results from the experiment, part of the laser energy is Raman-shifted, which can be seen in Fig. 4(a). The modulations appear at the lower side of the 2ω base frequency. Since $\omega_p \sim 0.1\omega$, the modulations appear first at $(2 - 0.1)\omega = 1.9\omega$, and then they are shifted to lower frequencies and side scattered. Also, as shown in the inset in Fig. 4(a), the simulated laser near field is more spread out in the case without a channel than when propagating through a channel, similar to the experiment.

To now address the electron acceleration due to FSRS, Fig. 4(b) shows that we observe stronger electron acceleration in the case without a channel. It is clearly reduced in the channel case. The transverse electron phase space shown in Fig. 4(c) reveals that the electrons are produced with a lower divergence in the presence of a channel. Following previous experiments demonstrating correlation between the FSRS and electron beam angular structures [25], this corresponds well to the observation of Figs. 3(f) and 3(g).

In conclusion, we have shown that the presence of preformed hollow density channels improves the propagation of short, ultraintense laser pulses in an inhomogeneous FI-relevant coronal plasma. The next step will be to apply this scheme of a predrilled channel to a FI target without a cone in large-scale experiments.

We acknowledge the expert support of the LULI laser team and fruitful discussions with S. N. Chen and A. Pinteau. This work was supported by Grant No. E1127 from Région Ile-de-France, UNR under DOE/NNSA Grant No. DE-FC52-06NA27616 and OFES/NNSA Grant No. DE-PS02-08ER08-16, Italian PRIN-20072KW45J, and HiPER-STFC.

*julien.fuchs@polytechnique.fr

[1] C. G. R. Geddes *et al.*, Phys. Rev. Lett. **95**, 145002 (2005).
[2] S. Sebban *et al.*, Phys. Rev. Lett. **86**, 3004 (2001).
[3] M. Tabak *et al.*, Phys. Plasmas **1**, 1626 (1994).
[4] K. Tanaka *et al.*, Plasma Phys. Controlled Fusion **46**, B41 (2004); Phys. Plasmas **7**, 2014 (2000).
[5] Y. Kitagawa *et al.*, Phys. Rev. E **71**, 016403 (2005).
[6] A. Lei *et al.*, Phys. Plasmas **16**, 056307 (2009).
[7] N. Naumova *et al.*, Phys. Rev. Lett. **102**, 025002 (2009).
[8] Y. Sentoku *et al.*, Fusion Sci. Technol. **49**, 278 (2006).
[9] R. Kodama *et al.*, Nature (London) **418**, 933 (2002); Y. Sentoku *et al.*, J. Phys. IV **133**, 425 (2006).
[10] S. Baton *et al.*, Phys. Plasmas **15**, 042706 (2008).
[11] R. Stephens *et al.*, Phys. Plasmas **12**, 056312 (2005).
[12] G. Li *et al.*, Phys. Rev. Lett. **100**, 125002 (2008).
[13] P. Young and P. Bolton, Phys. Rev. Lett. **77**, 4556 (1996); M. Borghesi *et al.*, Phys. Rev. Lett. **78**, 879 (1997); J. Fuchs *et al.*, Phys. Rev. Lett. **80**, 1658 (1998).
[14] S.-Y. Chen *et al.*, Phys. Rev. Lett. **80**, 2610 (1998).
[15] P. Young *et al.*, Phys. Rev. Lett. **75**, 1082 (1995); V. Malka *et al.*, Phys. Rev. Lett. **79**, 2979 (1997).
[16] K. Krushelnick *et al.*, Phys. Rev. Lett. **78**, 4047 (1997).
[17] A. Mackinnon *et al.*, Phys. Rev. Lett. **80**, 5349 (1998).
[18] S. Atzeni *et al.*, Comput. Phys. Commun. **169**, 153 (2005).
[19] S. Atzeni *et al.*, Nucl. Fusion **49**, 055008 (2009).
[20] B. Wattellier *et al.*, Opt. Lett. **29**, 2494 (2004).
[21] V. Malka *et al.*, Phys. Plasmas **4**, 1127 (1997).
[22] W. Kruer, *The Physics of Laser Plasma Interactions* (Westview Press, Boulder, CO, 2003).
[23] T. Antonsen and P. Mora, Phys. Rev. Lett. **74**, 4440 (1995); T. C. Chiou *et al.*, Phys. Plasmas **3**, 1700 (1996); G. Shvets and X. Li, Phys. Plasmas **8**, 8 (2001).
[24] Y. Sentoku and A. J. Kemp, J. Comput. Phys. **227**, 6846 (2008).
[25] X. Wang *et al.*, Phys. Rev. Lett. **84**, 5324 (2000).